An Investigation on the Metal Injection through the Producing of MIM-ed Low-Alloy Steel

S. Rezaei[1], A. Askari[2,*]

[1]Department of Materials Engineering, Science and Research Branch, Islamic Azad University, Tehran, Iran.
[2]Department of Mechanical Engineering, Nazarabad Centre, Karaj Branch,
Islamic Azad University, Karaj, Iran.
Received: 22 February 2024 - Accepted: 05 June 2024

Abstract

In this study, we demonstrate the injection stage of Metal Injection Molding (MIM) process to fabricate a small bend-type component. This non-standard but critical engine part is made of a feedstock from the low alloy steel 4605. To optimize various injection parameters, the five-variable Box-Behnken Design (BBD) is used with the assumption of a quadratic model, together with the statistical method of Response Surface Methodology (RSM). Samples are then fabricated, and their densities are measured. Hence, the significance of these factors as well as the mutual coupling between each two parameters are investigated using the analysis of variance (ANOVA). Finally, this paper reveals that injection temperature of 155 ◦C, the injection speed of 80 mm/s, holding pressure of 83 bar, holding time of 9 s and the injection pressure of 132 bar led to an optimum density of the green part, which becomes 4.892 g/cm^3. Then, a new sample is produced using these optimized settings, and the green component density is measured, which is extremely near to the predicted value. After sintering, the optimized sample's density and hardness are compared to the MIM-4605 standard criteria.

Keywords: Metal Injection Molding, Low Alloy Steel 4605, Feedstock, Density, Response Surface Methodology.

1. Introduction

Metal Injection Molding (MIM) is a cost-effective metallurgical technique to manufacture complex components [1]. MIM is composed of powder-binder mixing to make a feedstock, injection molding, debinding and finally sintering [2-4]. A great advantage of MIM process achieves a near net shaping, and provided that the production parameters are carefully adjusted, this leads to a product with high dimensional accuracy [3,5].
The feedstock is injected into the mold cavity to obtain a green part during the MIM process. Next, a catalyst or a solvent and thermal debinding technique is employed to remove the binder.
At last, the debinded part is sintered in a furnace [6-8]. What is important through all these steps is to optimize a broad range of parameters to achieve a product with excellent physical and mechanical properties, such as in density and strength [6].
So far, many efforts have so far been done on optimization of the MIM stages; for instance, the impact of injection parameters, such as green strength and the green part density have been investigated on the standard sample, which showed that mold temperature is the most critical parameter to achieve the best surface quality of the sample [4].
In [5], a range of optimal parameters for the injection stage of the stainless-steel powder (SS316L) feedstock have been obtained using Taguchi method, and it was revealed that the packing time has a high impact on the overall surface quality of the sample.
The low alloy steel 4605 is among MIM grades which has recently found great interest for manufacturing standard samples [9-12]. The 4605 alloy offers fairly high strength at a reasonable material cost in terms of its characteristics. Most studies on this alloy were focused on the impact of binder [13], alloy processing schemes [9] weighting percentage of the powder [12] and its rheological response in the mold [10-14].It was shown that by changing the production of the feedstock, one can fabricate samples with improved mechanical properties. Despite its attractive features, little attempt has been made to this alloy's parameter optimization when used in MIM. In fact, the relevant studies were mainly focused on standard samples and have not been adopted to a real engineering component experiencing substantially different fabrication situations. Practically, geometry and feedstock parameters play a role when using MIM [15].
Bend metallic components of small size are among wildly used parts in industrial engines [16]. They are appeared as hinges in communications and electronics [17]. A typical application of these metallic bends is in engines used in the automotive and the aerospace industry [6]. In terms of fabrication, various techniques are used to produce these components in large quantities. Among them, MIM is a promising technique which was reported for a range of alloys. In this study, we attempted to

*Corresponding author
Email address: ali.askari@kiau.ac.ir

produce a fairly complex bend-type engine component made of 4605 alloy possessing about 1mm-thickness via MIM process. We optimized key injection parameters in the MIM process using the Response Surface Methodology (RSM) technique. A broad range of parameters, including the injection pressure/ temperature/ speed, were evaluated on the optimal value of green part density. We fabricated a new sample based on the optimized parameters derived via the RSM technique and measured its density. The density and hardness of the sample after debinding and sintering were compared with the standard values disclosed for MIM-4605.

2. Materials and Methods

2.1. Materials

The initial material used in this study is the feedstock polyPOM 4605 B 341, provided by POLYMIM Company, Germany. This product is, in fact, the low alloy steel 4605. Fig. 1. shows the Scanning Electron Microscope (SEM) of this feedstock taken from VEGAIITESCAN. As can be observed, the particles are almost perfectly spherical and uniformly mixed with the binder, resulting in a unique particle size distribution in the feedstock. Consequently, the feedstock moldability is increased through the injection stage, while the final mechanical properties of sample are improved.

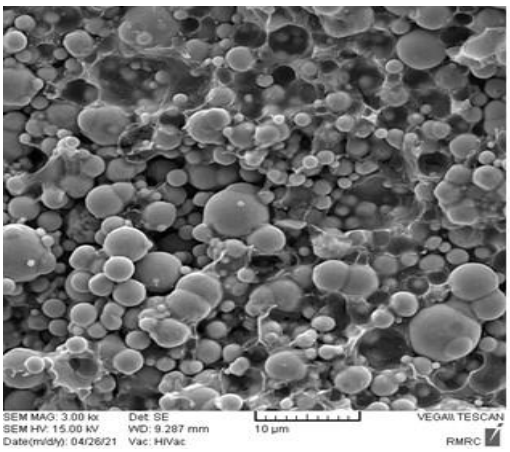

Fig.1. Scanning Electron Micrograph of feedstock polyPOM 4605 B 341.

2.2. Methods

The target component made via sheet metal forming is shown in Fig. 2(a). Besides, all dimensions are shown in millimeters inside the top and lateral views shown in Fig. 2(b). We aimed to fabricate this metallic component via MIM process.

For this, we made a two-cavity mold with the oversizing factor of %1.21 (This factor is taken according to the feedstock specifications announced by the provider). We have used the injection molding machine HTF60Wll HAITIAN ARAS through the injection process. To fabricate the sample, we then design a limited number of experiments, and for which, we characterize the injection parameters of the device. The experiments can be designed using the RSM tool based on a five-variable Box– Behnken Design (BBD) having six center-points and a quadratic model. The injection parameters constitute the RSM inputs- which are, in fact, the injection parameters - and are listed in Table. 1.

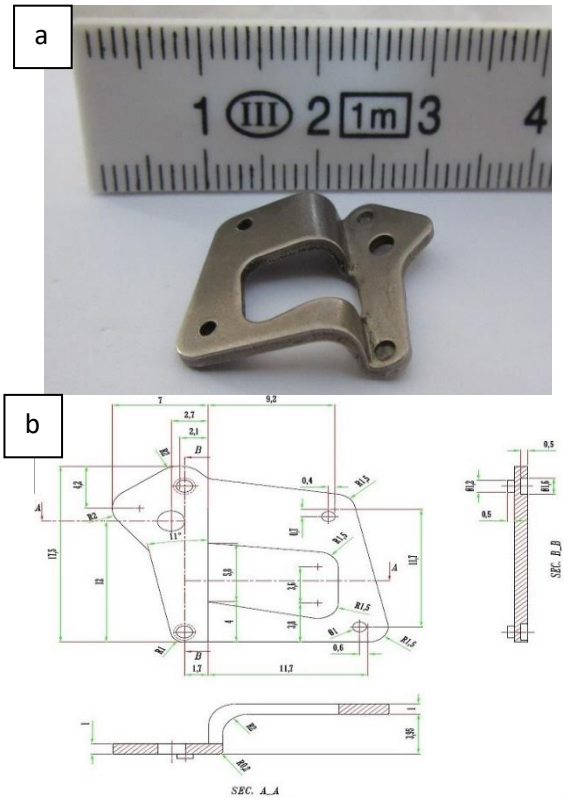

Fig. 2. (a)The target product to be fabricated via MIM process. Note that the sample is coated with a Chromium layer. (b) The target top and lateral views with dimensions in millimeter.

Table.1. Levels of the designed experiments.

No.	Variable		-1	0	+1
1	A	Injection temperature [°C]	140	155	170
2	B	Injection speed [mm/s]	30	60	90
3	C	Holding pressure [bar]	80	110	140
4	D	Holding time [s]	4	8	12
5	E	Injection pressure [bar]	90	115	140

The variation interval of inputs should be carefully chosen. To find a proper injection temperature interval for using the feedstock, we first perform two sets of analysis, i.e., the Differential Scanning Calorimetry (DSC) and Rheology analysis.The DSC analysis indicates the temperature behavior of the feedstock and shows the upper permitted temperature via the injection stage. The apparatus

used in our DSC analysis is DSC200F3Maia with the standard ASTM D 3418-15. The variation of the measured DSC data is plotted as a function of temperature for the feedstock in Fig. 3. As seen, at 164◦ C the feedstock begins melting and at T = 173.2◦ C it eventually reaches the end of melting point. The next analysis is the Rheology one, which is a critical step for characterizing the viscosity of the feedstock before filling the mold in injection stage. Through the injection molding, the shear rate is from 100 to 10000 s−1 [18]. For a feedstock to be appropriate for injection molding, the viscosity is required to be below 1000 Pa. s in this interval [19]. To perform the Rheology analysis, we have used Instron Model 3211 capillary Rheometer. It enables us to estimate the lower margin of the injection temperature for which the viscosity lies in a suitable range (i.e. < 1000 Pa.s). With regard to the device settings, a die of 0.127 mm and a length of 50 mm is selected for the rheometer device. The shear rate of the device is set between 10 and 10000 s−1 and the feedstock is tested at the temperatures 140 ◦C, 155◦ C and 170 ◦C. The rest of key injection parameters, including injection speed and pressure, together with the holding time and pressure are specified according to the requirements of the injection machine. By knowing the variation interval of the RSM inputs, we use the BBD algorithm embedded in the RSM simulation tool provided by Design Expert 11.0.3.0 (STATEASE Inc., Minneapolis, USA). The model output is set to be the density of the green part.

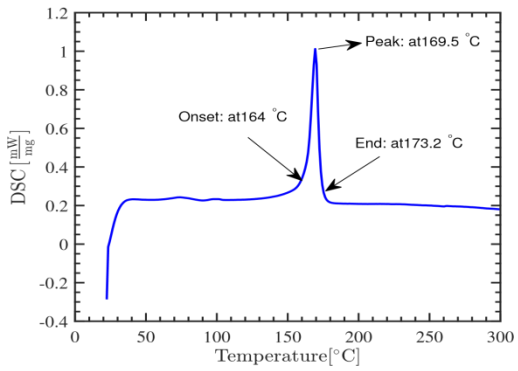

Fig.3. The DSC variation as a function of temperature for the selected feedstock.

By running the model, 46 experiments are designed as shown in Table. 2. according to the variable levels brought in Table. 1. Thus, we conduct the injection step of these experiments and determine the densities of the samples using the Archimedes technique and the MPIF 42 standard.

Following that, densities are loaded into the Design Expert in order to determine the optimal settings. We repeat the feedstock injection procedure, but this time using these adjusted parameters to obtain the most suitable green section. Then, debinding and sintering are performed on the green part. Note that, these processes are not the main purpose of this study, but in order to address the followed steps to fabricate the interested component, we briefly review these performed stages. The removal of the binder from the obtained green part is divided into two steps; first, catalytic debinding in which the samples are placed in Nitric acid HNO_3 of 100% purity at the temperature of 110◦C, with the N_2 atmosphere for 3 hours. Second, thermal elimination is performed whose cycle is designed according to thermogravimetrical analysis (TGA) [8].

The apparatus used for this purpose is TGA 209 F3Tarsus and the test is performed under the standard number ASTM E 1131-08. The TGA graph of the feedstock is shown in Fig. 4. in which weight reduction of the feedstock is obtained when heated at 10◦C/min and Nitrogen as a purge gas for the temperatures varying between 25 and 700◦C. To reduce the gaps between the powder particles, the sintering stage is performed at the temperature of 1250◦C for 2 hours [11,14]. Finally, the density and hardness of the sintered sample (The latter is measured by ROCKWELL HARDNESS TESTER LC series from FUTURE-TECH CORP, under the standard of ASTM E 18) are compared with their reported values for the 4605 low alloy steel. In addition, using the SEM images of the surface of sintered sample, its microstructure is studied in the next sections.

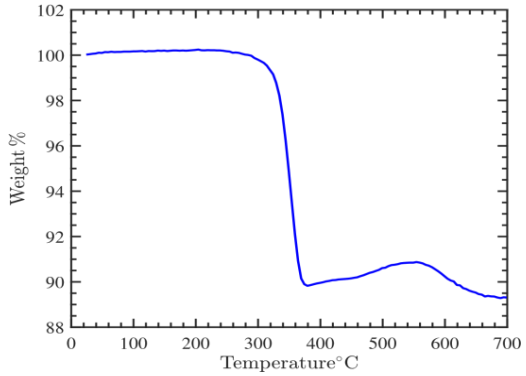

Fig.4. The thermogravimetrical analysis of the feedstock polyPOM 4605 B 341.

The removal of the binder from the obtained green part is divided into two steps; first, catalytic debinding in which the samples are placed in Nitric acid HNO_3 of 100% purity at the temperature of 110°C, with the N_2 atmosphere for 3 hours. Second, thermal elimination is performed whose cycle is designed according to thermogravimetrical analysis (TGA) [8].

Table.2. 46 designed tests via Box-Behnken technique, together with their experimental and predicted values of the green part densities.

Run	Std	A	B	C	D	E	Measured density [g/cm^3]	Predicted density [g/cm^3]
1	12	155	90	110	8	140	4.67	4.72
2	40	155	90	110	12	115	4.85	4.83
3	14	170	60	80	8	115	4.66	4.7
4	3	140	90	110	8	115	4.7	4.68
5	21	155	30	80	8	115	4.69	4.7
6	23	155	30	140	8	115	4.76	4.8
7	29	155	60	80	8	90	4.35	4.32
8	6	155	60	140	4	115	4.69	4.71
9	26	170	60	110	4	115	4.65	4.67
10	16	170	60	140	8	115	4.69	4.67
11	37	155	30	110	4	115	4.81	4.8
12	34	170	60	110	8	90	4.35	4.32
13	20	155	60	110	12	140	4.72	4.75
14	25	140	60	110	4	115	4.68	4.67
15	24	155	90	140	8	115	4.64	4.66
16	17	155	60	110	4	90	4.37	4.36
17	44	155	60	110	8	115	4.74	4.74
18	39	155	30	110	12	115	4.72	4.69
19	15	140	60	140	8	115	4.71	4.67
20	28	170	60	110	12	115	4.67	4.7
21	22	155	90	80	8	115	4.83	4.82
22	41	155	60	110	8	115	4.74	4.74
23	2	170	30	110	8	115	4.69	4.69
24	31	155	60	80	8	140	4.89	4.82
25	36	170	60	110	8	140	4.69	4.67
26	42	155	60	110	8	115	4.74	7.74
27	30	155	60	140	8	90	4.42	4.44
28	35	140	60	110	8	140	4.64	4.67
29	1	140	30	110	8	115	4.78	4.69
30	13	140	60	80	8	115	4.64	4.71
31	9	155	30	110	8	90	4.33	4.39
32	19	155	60	110	4	140	4.71	4.71
33	38	155	90	110	4	115	4.64	4.64
34	33	140	60	110	8	90	4.31	4.33
35	4	170	90	110	8	115	4.69	4.68
36	45	155	60	110	8	115	4.74	4.74
37	7	155	60	80	12	115	4.79	4.78
38	18	155	60	110	12	90	4.4	4.4
39	32	155	60	140	8	140	4.67	4.64
40	10	155	90	110	8	90	4.4	4.38
41	27	140	60	110	12	115	4.68	4.71
42	43	155	60	110	8	115	4.74	4.74
43	46	155	60	110	8	115	4.74	4.74
44	5	155	60	80	4	115	4.75	4.74
45	8	155	60	140	12	115	4.75	4.74
46	11	155	30	110	8	140	4.72	4.73

3. Results and Discussions

3.1. Feedstock Rheology

Rheology analysis is essential to ensure the steady flow of the process and to enable uniform filling to the mold cavity [20,21]. From Fig. 5, the viscosity of the feedstock's is decreased by increasing the shear rate; this shows that the feedstock has a pseudoplastic behavior [22]. This feature facilitates the injection molding to reduce the energy required for cavity filling [23]. The relation between shear rate and viscosity in a pseudo-plastic material is defined by Eq (1):

$$\eta = k\gamma^{n-1}, \quad \text{Eq. (1).}$$

where η and γ are the viscosity and shear rate, respectively, k is a constant and ηis the flow index [24,25]. The values of ηat the temperatures 140°C, 155° C, 170° C mentioned in section 2.2 - are 0.5309, 0.3668, 0.1050, respectively. Note that the flow index above 1 implies that the material is dilatant [26]. In addition, the flow index near 1 is not suitable for MIM process [11].

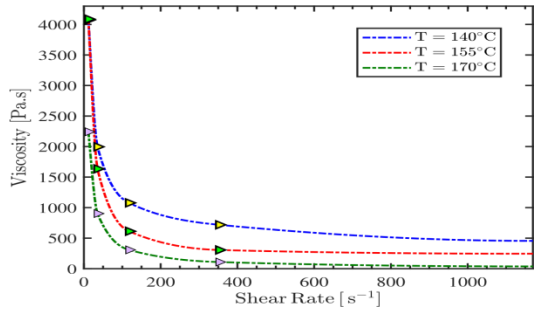

Fig.5. The viscosity of the sample as a function of shear rate at the temperature 140°C, 155° C, 170° C.

3.2. Optimization of the Designed Experiments

We mentioned that 46 experiments are designed in the RSM tool, as listed in Table. 2. The measured density of the green part are shown in the table (i.e. the actual density). We next derive a formula for the green part density as a function of RSM inputs using the BBD algorithm. Given that numerous factors have a minimal effect on the green component density, we next use analysis of variance to determine the relevant parameters (ANOVA). Table. 3. shows the corresponding data, in which the p-values indicate whether a model term is significant or not; i.e. those model terms with p-values less than 0.1 are identified as significant ones. Consequently, the terms C, D, E, BC, BD, CE, A^2 and E^2 belong to the significant terms category. The ultimate density of the green part - after removing the trivial terms - takes the following form Eq. (2):

$$\text{Density} = 4.74 - 0.0031A - 0.005B - 0.0169C + 0.0175D + 0.1737E - 0.065BC + 0.075BD - 0.0725CE - 0.0559A^2 - 0.1884E^2. \quad \text{Eq. (2).}$$

The positive signs for the model terms refer to the synergistic effect and the negative one shows the antagonistic effect [27]. The density obtained with this relation is shown as the predicted value in Table. 2. The other column in the table reports the measured density for each experiment. It can be seen that the two densities are well close together for the experiments, which shows that Eq. 2. is a suitable approximation to predict the green part density.

Now, the validity of the obtained equation for the density of the green part is examined. For this, the R2 is a proper criterion, which is the ratio of the sum of squares due to regression to the total sum of squares. The R value is at most 1 and indicates the validity of approximations for the density equation.

Thus, it refers to the case that there is a very good agreement between the experimental and the predicted value from the model [28]. The Predicted R2 of 0.8645 is in reasonable agreement with the Adjusted R2 of 0.9390; i.e. the difference is less than 0.2 which implies that our approximated expression for the green part density is valid. In other words, the variance of errors is less than those due to the dependent variables. These data are listed in Table. 4.Now, we have verified the obtained expression for the green part density.

Next, based on Eq. 2. we compute the optimum injection parameters to maximize the density of the green part. The obtained parametric values are tabulated in Table. 5. Then, according to these optimal injection parameters the fabrication procedure is again performed, and the final sample was realized. By measuring the density of this sample, the density was found to be 4.9 g/cm^3, which is very close to the typical value that was expected for ferrous-based feedstock [18]. The fabricated sample and its microscopic image are shown in Fig.6.(a) and Fig. 6.(b). As can be observed, the sample is free of defects on its surface, and the SEM picture demonstrates that the density is rather uniform, indicating that the binder is dispersed evenly throughout the full powder particles.

3.3. Effect of Injection Parameters on the Green Density

This section provides a detailed analysis of the effect and contribution of various injection parameters on the green part density. In finding the optimal parameters, we set the goal to be maximum density. However, it was generally expected to observe defects in a number of tests.

We address these issues and explore likely reasons. In addition, based on Eq. (2). some of these parameters have mutual effects on the density, while others can independently make a change in the density. We look at those mutual effects that play a role in realizing the optimal sample.

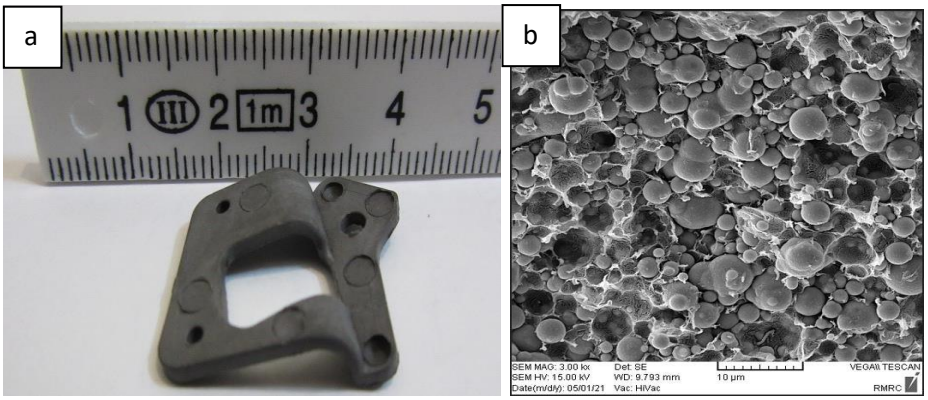

Fig. 6. (a) The fabricated green part realized according to the optimal injection parameters. (b) The SEM image of green part shown in (a).

Table. 3. Analysis of variance of regression coefficients of models.

Source	Sum of Squares	df	Mean Square	F-value	p-value
Model	0.9295	20	0.0465	35.64	0.0001
A-Injection temperature	0.0002	1	0.0002	0.1198	0.7321
B-Injection speed	0.0004	1	0.0004	0.3068	0.5846
C-Holding pressure	0.0046	1	0.0046	3.49	0.0733
D-Holding time	0.0049	1	0.0049	3.76	0.0639
E-Injection pressure	0.483	1	0.483	370.47	0.0001
AB	0.0016	1	0.0016	1.23	0.2785
AC	0.0004	1	0.0004	0.3068	0.5846
AD	0.0001	1	0.0001	0.0767	0.7841
AE	0	1	0	0.0192	0.891
BC	0.0169	1	0.0169	12.96	0.0014
BD	0.0225	1	0.0225	17.26	0.0003
BE	0.0036	1	0.0036	2.76	0.1091
CD	0.0001	1	0.0001	0.0767	0.7841
CE	0.021	1	0.021	16.13	0.0005
DE	0.0001	1	0.0001	0.0767	0.7841
A^2	0.0264	1	0.0264	20.25	0.0001
B^2	0.0001	1	0.0001	0.0418	0.8396
C^2	0.0001	1	0.0001	0.0744	0.7873
C^2	6.06E-06	1	6.06E-06	0.0046	0.9462
E^2	0.3068	1	0.3068	235.32	0.0001
Residual	0.0326	25	0.0013		
Lack of Fit	0.0326	20	0.0016		
Pure Error	0	5	0		
Cor Total	0.9621	45			

Table.4. The R2 values for the green part density equation.

Std. Dev.	**0.0361**	**R^2**	**0.9661**
Mean	4.66	Adjusted R^2	0.9390
C.V. %	0.7753	Predicted R^2	0.8645
		Adeq. Precision	20.9466

Table.5. Optimum parameter values for maximum density of the green part.

A	B	C	D	E	Density [g/cm^3]	Desirability
155	80	83	9	132	4.892	1

3.4. Injection Temperature

Fig. 7.(a) shows that by increasing the temperature, the density of the green part gradually increases to hit 4.74 g/cm^3, and then reduces.

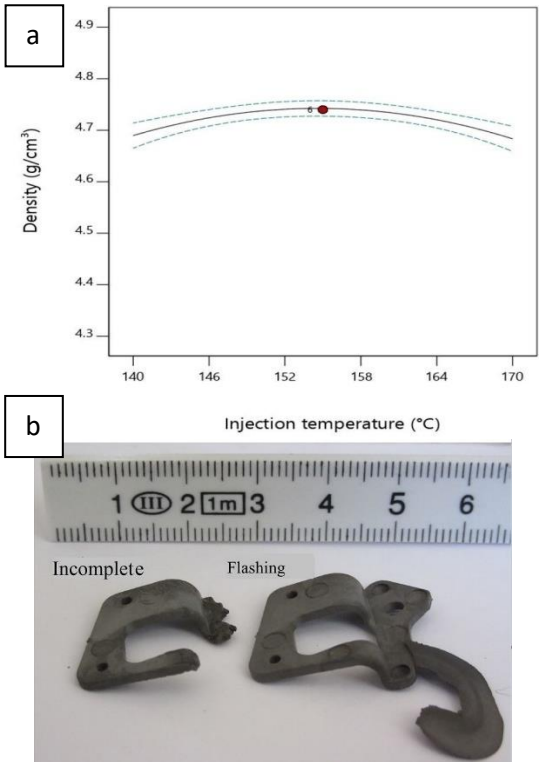

Fig. 7. (a)The density of the green part as a function of injection temperature. The green lines show the % 95 confidence interval. All other parameters are in their center values. (b) Two structures with incomplete filling and flashing. All other parameters are in their center values.

This is an interesting point as in [14], which was performed on a standard sample of 4605 alloy, the density steadily increases due to the temperature. We observed this behavior in a range of experiments; for instance, in run number 19 of Table. 2. the temperature was set at 140◦ C and the final sample had flashing; Or in run number 10 performed under the temperature of 170◦ C and similar injection parameters as in run number 19, an incomplete filling of the sample is observed as shown in Fig. 7.(b).

With regard to the sample with flashing occurred at a rather low temperature in run number 19, the reason is a high holding pressure of 140 bar applied to the sample [29].

For the case of an incomplete sample, at high injection temperature the feedstock flow is rapid. Since the gate thickness (Gate is the point at which the flow enters the mold) is small, the flow becomes frozen and leads to an incomplete sample.

Thus, the injection temperature is a function of feedstock, the sample geometry and the design of the mold and gate [15].

3.5. Injection Pressure

Fig. 8 shows that the density first increases by the pressure until reaching its maximum value at the pressure 127 bar. Afterward, it is gradually reduced and finally takes the value of 4.73g/cm^3 at the pressure 140 bar. Similar behavior was reported for the stainless-steel powder ss316L in [4]. Despite this, for the standard sample of 4605 alloy the density experiences a steady increase with the injection pressure [14].

Thus, high injection pressure does not necessarily lead to a higher density. This point can be understood by comparing runs 25 and 28 in Table. 2.; in both tests the injection pressure is high (i.e. 140 bar), but the run number 28 has a lower injection temperature; therefore, its density is slightly decreased. Large injection pressures also lead to defects. For instance, in run 28 we observed a defected sample, which is shown in Fig. 9.(a). As can be seen, the sample has flow marks on its surface.

This occurs when the injection temperature is low and the injection pressure is high at the same time [30].

As another case, consider the run number 39, with again low injection temperature and high injection pressures. As noted in [31], these conditions have led to surface wrinkles on samples, and we observed this as shown in Fig.9.(b) in run number 39.

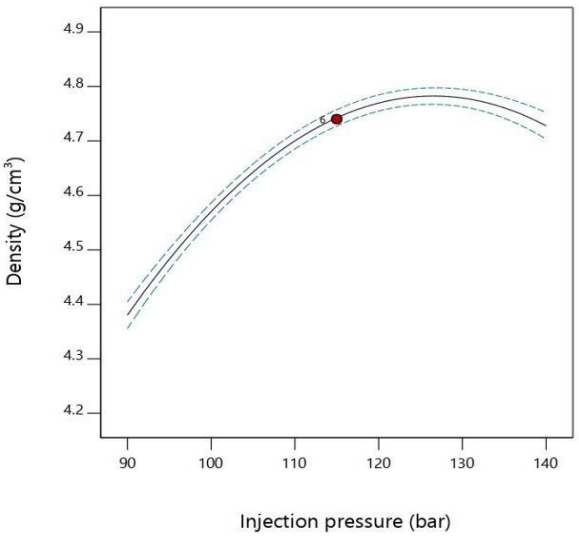

Fig.8. Variation of green part density as a function of injection pressure (All other parameters are in their center values).

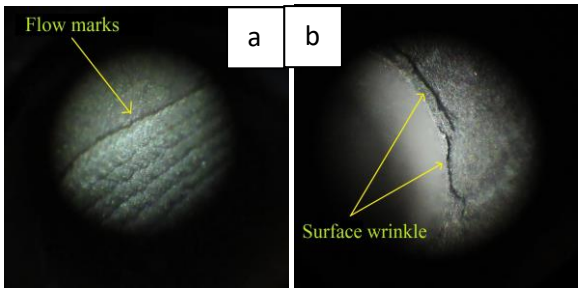

Fig. 9. Microscopic images of a green part surface when (a) flow marks and (b) surface wrinkle appear.

3.6. Holding Time

Fig. 10. shows the variation of density as a function of the holding time, which shows a gradual increase. This is because the feedstock is cooled down longer under pressure in the mold, which leads to a higher density. This effect is observed in the fabricated samples; Fig.11.(a) and Fig.11.(b).

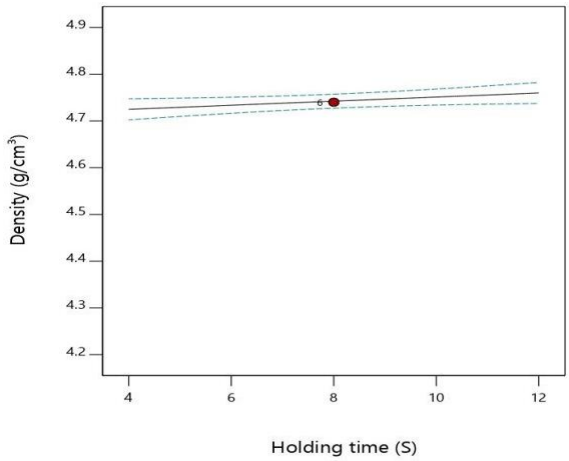

Fig. 10. The green part density as a function of holding time (All other parameters are in their center values).

show the SEM images of the two runs of 8 and 45, respectively in which only the holding time varies between the two. It is clear that the distribution of the powder particles and the binder is rather more homogeneous so that porous is reduced at run 45 – with a higher holding time.

This parameter also has a mutual coupling with the injection speed. As can be seen in Fig. 12., highest density occurs when both injection speed and holding time are high. This can be explained as follows. Before melted feedstock becomes solid inside the runner and gate, a large volume of the melted material is injected within the cavities, leading to a higher densities sample.

It happened in run numbers 2 and 18, where at a large holding time of 12 s, by increasing the injection speed from 30 to 90 mm/s, the density has grown from 4.72 to 4.85 g/cm^3.

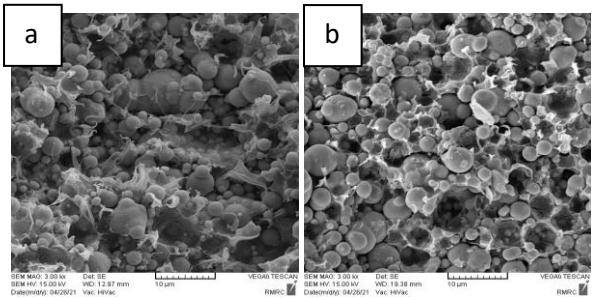

Fig. 11. The SEM image taken from the fabricated samples in run number 8 (a) and 45 (b).

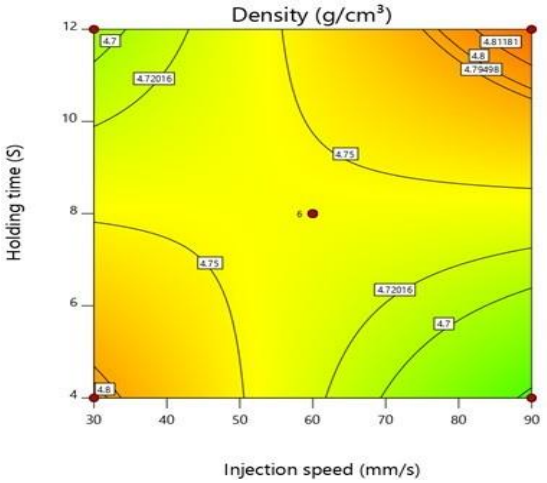

Fig. 12. The density contour of two mutual parameters of injection speed and holding time when all other parameters take their center values.

3.7. Injection Speed

According to the statistical models extracted from ANOVA (i.e. P values in Table**.** 3**.**) the impact of injection speed is negligible, and this can be seen in Fig**.**13**.**(a). However, the mutual effect of this parameter with other factors is significant. For instance, the mutual effect of injection speed and holding time on the green part density was shown in the contour of Fig**.** 12**.**; it was found that the density will get its maximum point when both these parameters have their highest values. With that in mind, in Fig**.**13**.**(b) we have shown the contour of density as a function of injection speed and holding pressure assuming the holding time takes its maximum value (i.e. 12 s). As can be seen, the holding pressure needs to be at its smallest value (i.e. 80 bar) while the injection speed is taking its maximum, to achieve higher density.

Hence, we can prevent formation of various defects due to solidification of feedstock before the complete filling of the cavity.

This point is expected as for a thin sample, in which there is no need for a high holding pressure [29]. It was practically observed in run number 21 where the density has reached a large density of 4.83 g/cm^3.

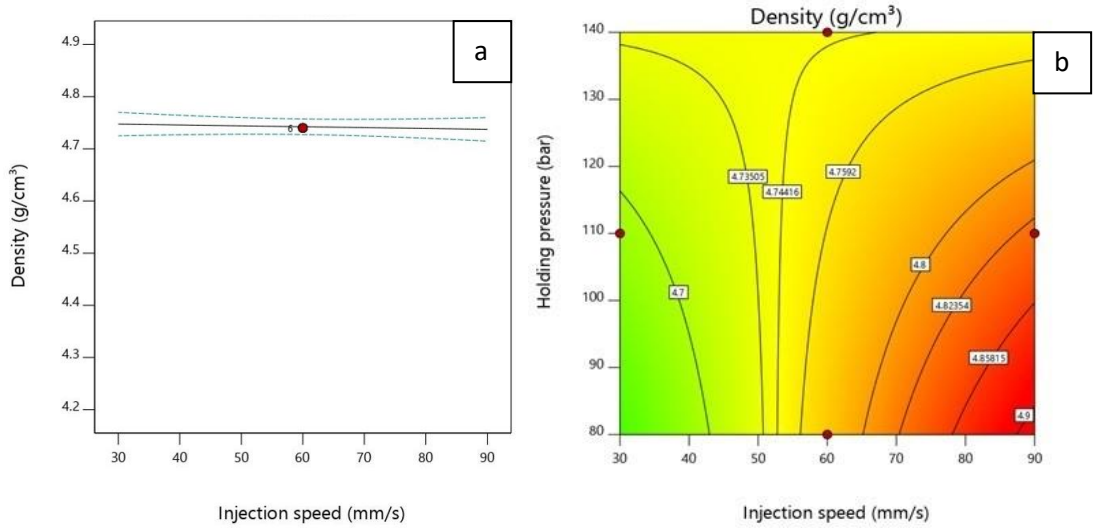

Fig.13. (a) The density of the green part as a function of injection speed. (b) The density contour of two mutual parameters of injection speed and holding pressure when holding time is set at 12 seconds and the remaining parameters takes their center values.

3.8. Holding Pressure

Fig. 14. shows the variation of the green part density with the mutual effect of holding pressure and the injection pressure. As can be seen, the density is gradually decreased by increasing the holding pressure, and the reduction rate has grown at higher injection pressures. Note that theholding pressure has also a mutual effect with injection speed, this has been explained in the previous section. The designed runs number 15 and 21 in Table. 2., wherein only holding pressure varies while other parameters are unchanged, show the effect of this parameter; By comparison, it can be seen that the density is reduced – from 4.84 to 4.63 g/cm^3 - when increasing the holing pressure. The physical behavior can be interpreted as follows: Since this downward trend of variation is different from the results reported in previous studies [14] and highlights the significant impact of sample geometry on optimization of the density, as explained in [15].

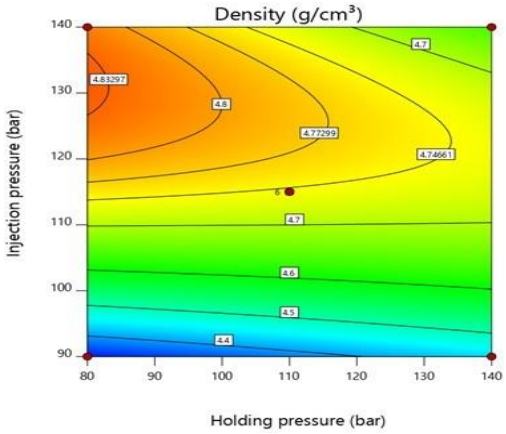

Fig.14. The density contour of two mutual parameters of injection pressure and holding pressure when the remaining parameters have their center values.

3.9. Fabrication of Sintered Part

Fig. 15.(a) shows the sample after being sintered. As can be seen, there is no apparent defect on the surface. The average hardness measured on the sample reaches 61 HRB and the density is 7.52 g/cm^3; These values are in agreement with the standard values reported for the metal injection molded MIM-4605 (under the code ASTM B 883-05) and validate the effectiveness of the performed optimization.

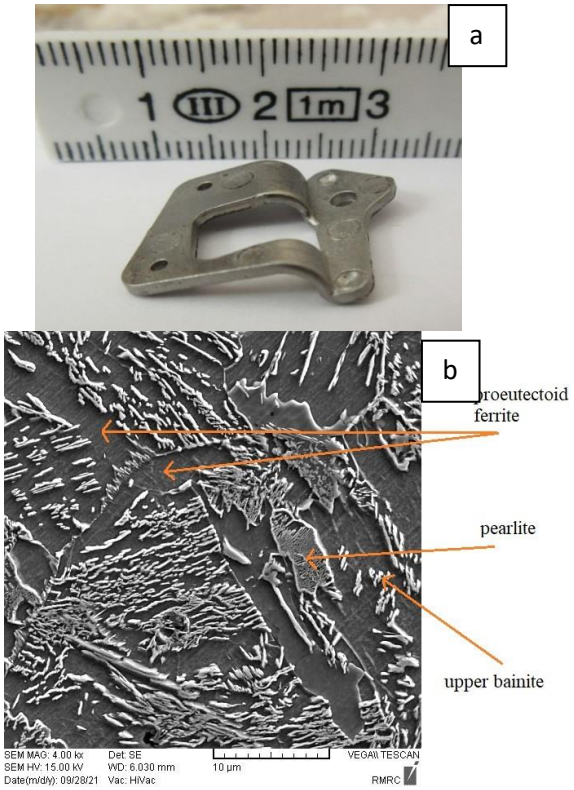

Fig.15. (a) The final fabricated sample after sintering. (b) The SEM image of the sintered sample.

The physical and mechanical properties of the 4605 relied primarily on microstructure. The microstructure of the sintered part shows a homogeneous distribution of the phases in the matrix, as indicated in Fig. 15.(b). As can be seen, the proeutectoid ferrite consists of most parts of the sample, while pearlite and upper bainite phases rarely appear on their surface.

4. Conclusion

1. In this study, we investigated the optimum injection parameters to fabricate a fairly bend-type component made of a feedstock from the low alloy steel 4605, that is frequently used in industrial engines.
2. Using Response Surface Methodology and assuming the injection temperature, injection speed, holding pressure, holding time and injection pressure, the Box-Behnken Design(BBD) - with these five variables - were employed in a quadratic model to design experiments.
3. We statistically investigated these experiments to reach a unique expression for green part density as a function of those parameters. After evaluating the resulting density equation, it was determined that an injection temperature of 155° C, an injection speed of 80 mm/s, a holding pressure of 83 bar, a holding duration of 9 s, and an injection pressure of 132 bar provide the optimum value for the green component density.
4. Then, we fabricated a new sample based on these conditions and reached 4.9 g/cm^3, which was close to the reported values for the parts. By comparing the measured density and hardness of the sample after debinding and sintering - with the standard values reported for MIM 4605, under the code B 883-05, we found a very good agreement.

References

[1] Husein, S., Park, J.H., Choi, D.Y. and Ko, Y.G., Influence of sintering temperature on microstructure and mechanical properties of Fe–2Ni–2Cu alloy processed by metal injection moulding. Mater. Res. Innov. 2014; 18(sup2):S2-633.
[2] Huang, C., Li, L., Ngai, T., Zhang, W. and Ngai, S., November. Effect of sintering temperature and solution treatment on microstructure and mechanical properties of high-N Ni-free austenitic stainless steel prepared by metal injection molding. Mater. Res. Express. IOP Publishing. 2020; 1676(1):012099
[3] Berginc, B., Kampus, Z., Sustarsic, B. The use of the TAGUCHI approach to determine the influence of injection-moulding parameters on the properties of green parts. J. Achieve. Mater. Manuf. Eng. 2006;15(1-2):63–70.
[4] Chua, M.I.H., Sulong, A.B, Abdullah, M.F., et al. Optimization of injection molding and solvent debinding parameters of stainless–steel powder (ss316l) based feedstock for metal injection molding. Sains Malays. 2013; 42(12):1743–50.
[5] Arifin, A., Sulong, A.B., Muhamad, N. Optimizing injection parameter of metal injection molding processes using the feedstock of 16 μm stainless steel powder (ss316l), peg, pmma and stearic acid. J. Appl. Sci. Res. 2012; 8(6):2998-3003
[6] Jamaludin KR, Muhamad N, Rahman MA, Amin SY, Ahmad S, Ibrahim MH. Sintering parameter optimisation of the SS316L metal injection molding (MIM) compacts for final density using taguchi method. InUniv Consort Symp 2009 pp. 258-62.
[7] Virdhian S, Osada T, Kang HG, Tsumori F, Miura H. Evaluation and analysis of distortion of complex shaped Ti-6Al-4V compacts by metal injection molding process. Key Eng. Mater. 2012, 19;520:187-94.
[8] Thomas-Vielma P, Cervera A, Levenfeld B, Várez A. Production of alumina parts by powder injection molding with a binder system based on high density polyethylene. J. Eur. Ceram. Soc. 2008; 28(4):763-71.
[9] Coleman AJ, Murray K, Kearns M, Tingskog TA, Sanford B, Gonzalez E. Processing and properties of MIM AISI 4605 via master alloy routes. In Advances in powder metallurgy & particulate materials-2012: proceedings of the 2012 international conference on powder metallurgy & particulate materials sponsored by the Metal Powder Industries Federation, 10-13, Nashville, TN 2012 (pp. 4-35). Metal Powder Industries Federation Princeton.
[10] Askari A, Alaei MH, Mehdipoor Omrani A, Nekouee K, Park SJ.Rheological and thermal characterization of aisi 4605 low-alloy steel feedstock for metal injection molding process. Met. Mater. Int. 2020; 26(12):1820–9.
[11] Momeni, V., Zangi, H., Alaei, M.H. Effect of thermal debinding and sintering parameters on the mechanical properties of 4605 mim compact using the rsm. Adv. Mater. Process. Technol., 2021; 1:1–16
[12] Momeni V, Alaei MH, Askari A, Rahimi AH, Nekouee K. Effect of the fraction of steel 4605 powder in the load in injection molding with the use of a polymer-based binder. Met. Sci. Heat Treatment. 2020; 61:777-81.
[13] Momeni V, Askari A, Allaei MH, Zangi H. Investigating the effect of stearic acid on the mechanical, rheological, and microstructural properties of AISI 4605 feedstock for metal injection molding process. Trans. Indian Inst. Met. 2021; 74(9):2161-70.
[14] Momeni, V., Alaei, M. Optimization of injection parameters in metal injection molding of 4605 low alloy steel. Mod. Mech. Eng. 2019; 19(5): 1199–208.
[15] Ebel T. Metal injection molding (MIM) of titanium and titanium alloys. In Handbook of metal

Injection Molding, 2019; 1 (pp. 431-60). Woodhead Publishing.
[16] Omar MA, Subuki I, Abdullah N, Hassan N. Production of medical devices prototype through metal injection moulding technique. Mater. Res.Innov. 2009; 13(3):320-2
[17] Lin, K.H. 2011. Wear behavior and mechanical performance of metal injection molded fe–2ni sintered components. Mater. Des., 32(3): 1273–82.
[18] German RM. Injection molding of metals and ceramics. Powder Metall., 1997; 42:157-60.
[19] Hossain A, Choudhury IA, Nahar N, Hossain I, Bin Mamat A. Experimental and theoretical investigation of powder–binder mixing mechanism for metal injection molding. Mater. Manuf. Process. 2015; 30(1):41-6.
[20] Amin SY, Muhamad N, Jamaludin KR, Fayyaz A, Yunn HS. Characterization of the feedstock properties of metal injection-molded WC-Co with palm stearin binder system. Sains Malays. 2014; 43(1):123-8.
[21] Islam ST, Samanta SK, Lohar AK, Bandyopadhyay A. Rheological study of alumina feedstock for a micro-powder injection moulding application. Mater. Res. Express., 2019; 6(9):095204.
[22] Virdhian S, Doloksaribu M, Supriadi S, Balfas NM, Suharno B, Shieddieque AD. Characterization of 17-4 PH stainless steel metal injection molding feedstock using mixing torque data. In IOP Conference Series: Mater. Sci. Eng. 2020; 980(1):012053, IOP Publishing.
[23] Machaka R, Ndlangamandla P, Seerane M. Capillary rheological studies of 17-4 PH MIM feedstocks prepared using a custom CSIR binder system. Powder Technol. 2018; 15(326):37-43.
[24] Zakaria H, Muhamad N, Sulong AB, Ibrahim MH, Foudzi F. Moldability characteristics of 3 mol% yttria stabilized zirconia feedstock for micro-powder injection molding process. Sains Malays. 2014; 43(1):129-36.
[25] Ramli MI, Sulong AB, Muhamad N, Muchtar A, Arifin A. Stainless steel 316L–hydroxyapatite composite via powder injection moulding: rheological and mechanical properties characterisation. Mater. Res. Innov. 2014; 8(18):S6-100.
[26] Li D, Pan D, Zhang C, Wu W, Lu R, Yang Z. Powder injection moulding of Inconel 713C alloy. Powder Metall., 2019; 62(4):240-6.
[27] Sahu, J., Acharya, J., Meikap, B., Optimization of production conditions for activated carbons from tamarind wood by zinc chloride using response surface methodology. Bioresour. Technol.2010; 101(6):1974–82.
[28] Mehdi H, Mishra RS. An experimental analysis and optimization of process parameters of AA6061 and AA7075 welded joint by TIG+ FSP welding using RSM. Adv. Mater. Process. Technol. 2022; 8(1):598-620.
[29] Heaney DF, Greene CD. Molding of components in metal injection molding (MIM). In Handbook of Metal Injection Molding 2019;1 (pp. 105-27). Woodhead Publishing
[30] Hwang KS. Common defects in metal injection molding (MIM). In Handbook of Metal Injection Molding 2012;1 (pp. 253-69). Woodhead Publishing.
[31] Mohamad NN, Muhamad N, Jamaludin KR, Ahmad S, Ibrahim MH. Flow behavior to determine the defects of green part in metal injection molding. Int. J. Mech. Mater. Eng., 2009; 4(1):70-5.